A Robust Automatic Method for Removing Projective Distortion of Photovoltaic Modules from Close Shot Images

Yu Shen[1], Xinyi Chen[1], Jinxia Zhang[1,*], Liping Xie[1], Kanjian Zhang[1]

and Haikun Wei[1,*]

[1] Key Laboratory of Measurement and Control of CSE, Ministry of Education, School of Automation, Southeast University, Nanjing 210096, PR China

jinxiazhang@seu.edu.cn
hkwei@seu.edu.cn

Abstract. Partial shading and hot spots may cause power loss and sometimes irreversible damage of photovoltaic (PV) modules. In order to evaluate the power generation of PV modules, it is necessary to calculate the area of shading and hot spots. The perspective distortion makes region closer to the camera have more pixels, which results in misestimate of shading area and hot spots. To solve this problem, a robust automatic method for removing projective distortion of photovoltaic modules from close shot images is proposed in this paper. Firstly, Images are converted to gray scale, and their edges are detected by Canny algorithm. Then, lines are detected by Hough transform, vanishing points are found by intersecting lines, and the line at infinity is specified by vanishing points. Next, the projective transformation matrix is decomposed into an affine transformation matrix and a simple projective transformation matrix, which has only two degrees of freedom. Affine rectification is derived from computing this simple projective transformation matrix, and finally, right angles are recovered by computing shear transformation matrix. The close shot visible and infrared images are collected for experiments. The results show that the proposed method performs better on rectification of PV modules from close shot images.

Keywords: Projective Distortion, Photovoltaic, Affine Rectification.

1 Introduction

The field of photovoltaics has developed rapidly in recent years. In the operation of photovoltaic power station, partial shading [1][2] and hot spots [3][4] usually occur, and reduces the PV module output power. In order to evaluate the power loss caused by shading and hot spots of different types, different locations and different areas, it is feasible to take close shot images of photovoltaic (PV) modules, then combine

computer vision [5][6], pattern recognition [7], and machine learning [8] methods, to recognize the photovoltaic modules, shading and hot spots in the image. Object detection [9][10], semantic segmentation [11]-[14], and salient analysis [15][16] offer fruitful methods, but problems of projective distortion still remain. Projective distortion makes parallel lines in the real world imaged as converging lines and region closer to the camera occupy more pixels than those farther away.

In order to estimate the area of shading and hot spots, projective distortion of photovoltaic modules should be removed from the images. A common approach is to recognize a rectangular object in the real world and find its four corners in the image. It is possible to compute the transformation matrix and "undo" the projective distortion by the inverse transformation [17]. This method depends on the corners and the corners are usually need to be located manually. An automatic way to find corners can be realized by detecting and segmenting the rectangular object, which may cause deviation of corners and errors of transformation matrix. TILT [18] extracts a class of "low-rank textures" in a 3D scene, and automatically rectifies the texture in a 3D scene from user-specified windows in 2D images. TPS [19] rectifies objects by training a spatial transformer network to find the position of fiducial points. GCO [20] adopts a frequency approach for affine rectification of planar homogeneous texture, which manifests as regular repeating scene elements along a plane. Some works rectify images based on morphological analysis or registration techniques [21-23]. These methods are universal for various scenes and objects, but there is a paucity of work specially designed for PV modules rectification. Some existing methods may rectify inaccurately when the corners or edges of PV modules are covered.

The motivation of this paper is to propose a robust automatic method for removing projective distortion of photovoltaic modules from close shot images. The contribution of our work is: 1) creating a database for close-shot visible and Infrared (IR) images; 2) proposing a rectification method that makes full use of texture information of PV modules. Compared to existing methods, the proposed approach is more robust and performs well even if the corners or edges of PV modules are covered. Besides, the proposed method does not rely on a large amount of training samples, thus can be used for distributed PV stations with a small number of samples.

Firstly, 100 visible images and 600 infrared images are collected. The images are taken from close shot, thereby contain sufficient texture information of PV modules. Secondly, images are converted to gray scale and edges are detected by Canny algorithm [24]-[26]. Thirdly, lines are detected by Hough transform [27], vanishing points are specified, and the line at infinity is found. Next, the projective transformation matrix is decomposed into an affine transformation matrix and a simple projective transformation matrix, which has only two degrees of freedom. Then, affine rectification is conducted by computing this simple projective transformation matrix. Finally, right angles are recovered by computing shear transformation [28] matrix.

The rest parts of this paper are organized as follows: in section 2, a robust automatic method for removing projective distortion of photovoltaic modules is

proposed; the experiments and results are shown in section 3 and conclusions are drawn in section 4.

2 Method

In this section, a robust automatic method for removing projective distortion of photovoltaic modules from close shot images is described in detail. The framework is shown as Fig.1. The projective transformation is decomposed as a simple projective transformation and an affine transformation. The affine transformation can be further decomposed as a shear transformation and other three transformations (translation, rotation and scale).

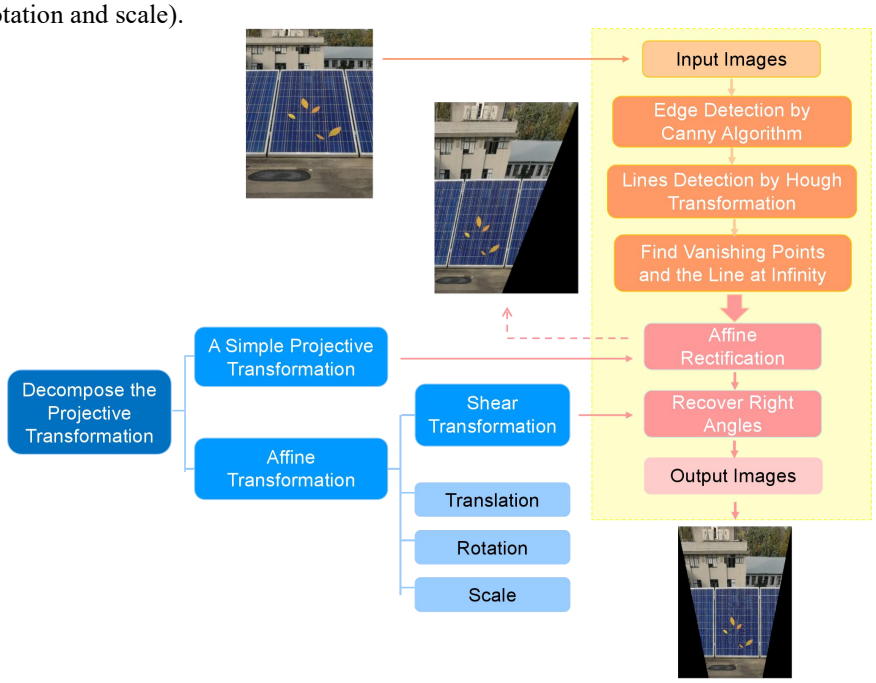

Fig. 1. The framework for removing projective distortion of photovoltaic modules

2.1 Decomposition of the Projective Transformation

A projective transformation can be represented by a homogeneous matrix $\mathbf{H}$: $\mathbf{x}' = \mathbf{H}\mathbf{x}$. The point is specified by a homogeneous vector $\mathbf{x} = (x_1, x_2, x_3)^{\mathrm{T}}$, and the projective transformation is shown more detailedly as follows:

$$\begin{pmatrix} x_1' \\ x_2' \\ x_3' \end{pmatrix} = \begin{bmatrix} h_{11} & h_{12} & h_{13} \\ h_{21} & h_{22} & h_{23} \\ h_{31} & h_{32} & h_{33} \end{bmatrix} \begin{pmatrix} x_1 \\ x_2 \\ x_3 \end{pmatrix} \tag{1}$$

Where $\mathbf{H}$ is a non-singular 3-order square matrix. The projective transformation will not be changed if each element of $\mathbf{H}$ is multiplied by a non-zero factor, because the

matrix $\mathbf{H}$ is homogeneous. That is, $\mathbf{H}$ has eight degrees of freedom, and h_{33} can be set as 1, thus a projective transformation can be decomposed as follows:

$$\mathbf{H} = \mathbf{H}_{\mathrm{P}}\mathbf{H}_{\mathrm{A}} = \begin{bmatrix} 1 & 0 & 0 \\ 0 & 1 & 0 \\ v_1 & v_2 & 1 \end{bmatrix} \begin{bmatrix} a_{11} & a_{12} & a_{13} \\ a_{21} & a_{22} & a_{23} \\ 0 & 0 & 1 \end{bmatrix} \tag{2}$$

Where $\mathbf{H}_{\mathrm{A}}$ is a affine transformation, which has six degrees of freedom. After an affine transformation, the parallel lines are mapped to parallel lines and ratio of areas remains unchanged. While $\mathbf{H}_{\mathrm{P}}$ is another projective transformation, which has only two degree of freedom.

Therefore, we can recover the affine properties of photovoltaic module if $\mathbf{H}_{\mathrm{p}}$ is known.

2.2 Affine Rectification

Affine rectification can be applied to the image to recover the affine properties, such as the parallel lines in the world plane are still parallel in the image, and the ratio of areas in the world plane keep the same as the ratio in the image.

According to equation (2), we can recover the affine properties of photovoltaic module as follows:

$$\mathbf{x}_{\mathrm{A}} = \mathbf{H}_{\mathrm{P}}^{-1}\mathbf{x}_{\mathrm{P}} \tag{3}$$

Thus, the key problem of affine rectification is to calculate the matrix $\mathbf{H}_{\mathrm{P}}$.

A line in the plane is denoted by an equation $ax + by + c = 0$. Thus, we represent a line by the homogeneous vector $\mathbf{l} = (a, b, c)^{\mathrm{T}}$. After a projective transformation, parallel lines in the original plane may intersect in the projective plane. The intersections in the projective plane correspond to ideal points, or points at infinity in the original plane, which can be represented by homogeneous vectors $\mathbf{x} = (x_1, x_2, 0)^{\mathrm{T}}$ with last coordinate $x_3 = 0$. The set of all ideal points lies on a single line, known as the line at infinity, represented by the homogeneous vector $\mathbf{l}_{\infty} = (0,0,1)^{\mathrm{T}}$.

Under the point transformation $\mathbf{x}' = \mathbf{H}\mathbf{x}$, the line transform can be represented as:

$$\mathbf{l}' = \mathbf{H}^{-\mathrm{T}}\mathbf{l} \tag{4}$$

It can be proved that after the affine transformation $\mathbf{H}_{\mathrm{A}}$, the line at infinity remains the line at infinity. While after the projective transformation $\mathbf{H}_{\mathrm{P}}$, the line at infinity may correspond to a line represented as a homogeneous vector $\mathbf{l}'_{\infty} = (l_1, l_2, 1)^{\mathrm{T}}$:

$$\mathbf{l}'_{\infty} = \mathbf{H}_{\mathrm{P}}^{-\mathrm{T}}\mathbf{l}_{\infty} \tag{5}$$

That is:

$$\begin{bmatrix} 1 & 0 & v_1 \\ 0 & 1 & v_2 \\ 0 & 0 & 1 \end{bmatrix} \begin{pmatrix} l_1 \\ l_2 \\ 1 \end{pmatrix} = \begin{pmatrix} 0 \\ 0 \\ 1 \end{pmatrix} \tag{6}$$

v_1 and v_2 in matrix $\mathbf{H}_\mathrm{P}$ can be derived as follows:

$$\begin{cases} v_1 = -l_1 \\ v_2 = -l_2 \end{cases} \tag{7}$$

Therefore, we can get the matrix $\mathbf{H}_\mathrm{P}$ if the line $\mathbf{l}'_\infty$ has been found in the image.

2.3 How to find the Line at Infinity?

Firstly, RGB images are converted to grayscale. Secondly, edges are found by Canny edge detection algorithm. Thirdly, lines are detected by Hough transformation. (see Fig.6(b))

Hough transformation converts image space to parameter space. In the image space, each pair of x and y corresponds to a point, and a line is denoted by a pair of k and b:

$$y = kx + b \tag{8}$$

In the parameter space, each pair of k and b corresponds to a point, and a line is denoted by a pair of x and y:

$$b = -xk + y \tag{9}$$

That means lines and points are dual in the image space and parameter space. Thus, if many points lie on a line in the parameter space, it may represent that lines intersect at a vanishing point. The location of this vanishing point can be calculated by equation (9). (see Fig.7(a))

Parallel lines in the photovoltaic module has two directions (see Fig.4 and Fig.5), and we can recognize the line at infinity in the image in different conditions: 1) If parallel lines of each direction intersect respectively at a point in the image after projective transformation, the line at infinity in the image is simply the line through these two points (see Fig.2(a)). 2) If parallel lines of one direction intersect at a point, and parallel lines of the other direction keep parallel, the line at infinity in the image can be considered as the line through this point and parallels with these parallel lines in the image (see Fig.2(b)).

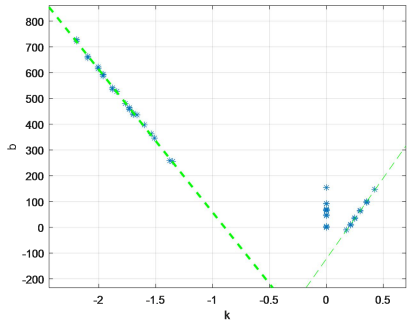

(a)

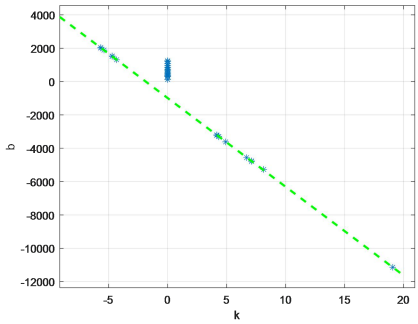

(b)

Fig. 2. Points in parameter space after Hough transformation (a) two lines in parameter space correspond to two vanishing points in image space; (b) a single line in parameter space corresponds to a single vanishing point in image space.

According to section 3.2, recognizing the line at infinity in the image $\mathbf{l}'_{\infty}$ make it possible to recover affine properties. (see Fig.6(c))

2.4 Recovery of Right Angles

Affine rectification is enough for area estimation of shading and hot spots. However, considering that the location of shading and hot spots also influence the power generation loss of PV modules, we can do one more step to recover the right angles of PV modules.

Right angles can be recovered by calculating shear transformation matrix $\mathbf{H}_{\text{sh}}$:

$$\mathbf{H}_{\text{sh}} = \begin{bmatrix} 1 & sh_y & 0 \\ sh_x & 1 & 0 \\ 0 & 0 & 1 \end{bmatrix} \tag{10}$$

sh_x denotes the shear factor along the x axis, and sh_y represents the shear factor along the y axis. (see Fig.3)

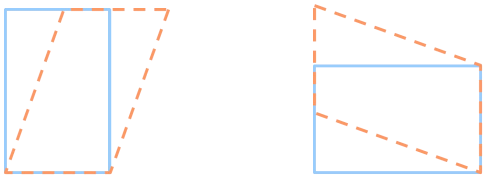

Fig. 3. Shear transformation (a) shear transformation along the x axis; (b) shear transformation along the y axis.

According to equation (4), suppose $\mathbf{l}$ is the line in the plane without shear transformation (see the blue rectangle in Fig.3), the corresponding line $\mathbf{l}'$ after shear transformation (see the orange parallelogram in Fig.3) satisfies:

$$\mathbf{H}_{\text{sh}}^{\text{T}}\mathbf{l}' = \mathbf{l} \tag{11}$$

Let $\mathbf{l}_{\text{a}} = (0,1,l_{3a})^{\text{T}}$ and $\mathbf{l}_{\text{b}} = (1,0,l_{3b})^{\text{T}}$ represent horizontal and vertical lines in PV module, the corresponding slope k of lines in the affine rectified image can be found by parameter space of Hough transformation (see Fig.7(b)). Then we can get $\mathbf{l}'_{\text{a}} = (k_a,-1,l'_{3a})^{\text{T}}$ and $\mathbf{l}'_{\text{b}} = (k_b,-1,l'_{3b})^{\text{T}}$. Solving equation (12) and (13), the shear transformation matrix can be calculated.

$$\mathbf{H}_{\text{sh}}^{\text{T}}\mathbf{l}'_{\text{a}} = \mathbf{l}_{\text{a}} \tag{12}$$

$$\mathbf{H}_{\text{sh}}^{\text{T}}\mathbf{l}'_{\text{b}} = \mathbf{l}_{\text{b}} \tag{13}$$

It can be proved that the shear transformation matrix is invertible. Thus, the right angles can be recovered (see Fig.6(d)) as follows:

$$\mathbf{x}' = \mathbf{H}_{\mathrm{sh}}^{-1}\mathbf{x} \tag{14}$$

3 Experiments

Data collection is described in section 3.1. Experiments for removing projective transformation distortion of PV modules are shown in section 3.2. In order to demonstrate the application value of our work, we also do one more step to estimate the area of shading and hot spots, shown in section 3.3.

3.1 Data Collection

We collect 100 close-shot visible images of photovoltaic modules in our photovoltaic experimental system. A cellphone is used to get visible images (1440 × 1080 pixels) on sunny days, as shown in Fig.4. The left image corresponds to a normal PV module, and other images show PV module with shading of leaves.

Fig. 4. Visible images of photovoltaic modules

600 infrared images (320 × 240 pixels) are provided by an enterprise specializing in manufacturing photovoltaic products. FLIR infrared camera was used to obtain the images on sunny days. Infrared images of photovoltaic modules are shown as Fig.5. The left column of images corresponds to normal PV module and other images show hot-spotted PV module.

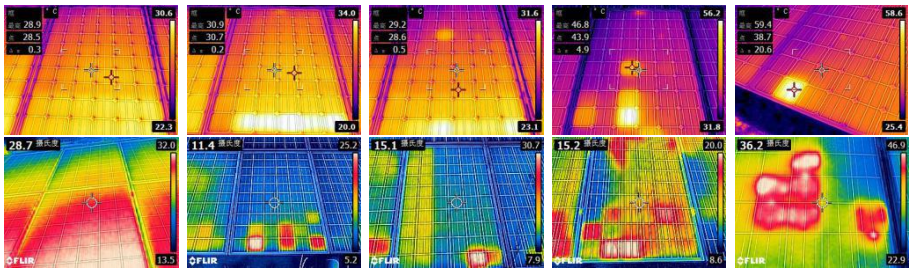

Fig. 5. Infrared images of photovoltaic modules

3.2 Removing Perspective Distortion of PV Modules

The results of the proposed method are shown in steps as follows: For an original image (see Fig.6(a)), firstly it was converted to grayscale. Edges are found by Canny edge detection algorithm and lines are detected by Hough transformation. (see Fig.6(b)) Affine properties are recovered as shown in Fig.6(c) and right angles are recovered as shown in Fig.6(d).

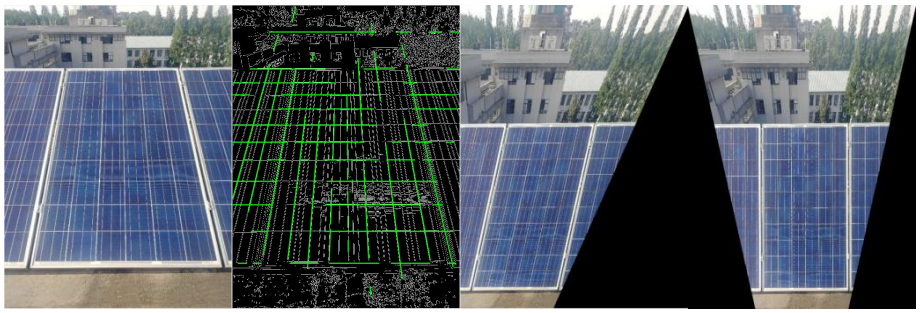

(a) (b) (c) (d)

Fig. 6. Removing projective distortion of photovoltaic modules (a) original image; (b) lines detection by Hough transformation; (c) affine rectification; (d) recovery of right angles.

Fig.7(a) shows how the vanishing point is specified. The green line in parameter space corresponds to a point in the image space, and this point is a vanishing point. Fig.7(b) shows the slopes of lines in Fig.6(c). We can see clearly that there are two main directions of lines.

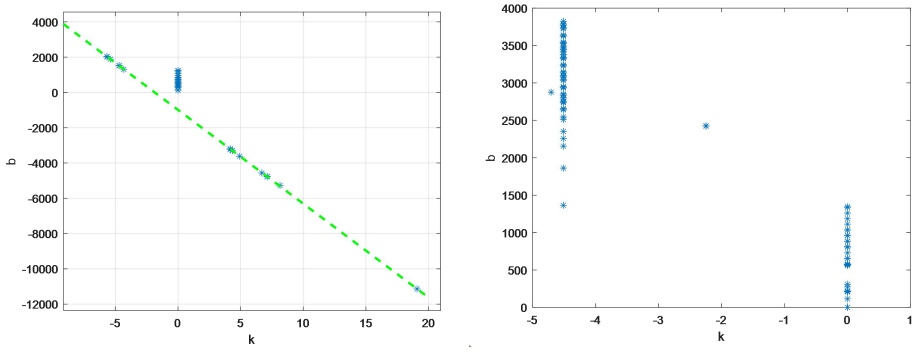

(a) (b)

Fig. 7. Points in parameter space after Hough transformation (a) points in parameter space of original image; (b) points in parameter space of affine rectified image.

Results for more images are shown as follows: Fig.8 displays the rectified visible images of PV modules corresponding to Fig.4, Fig.9 shows the rectified IR images of PV modules corresponding to Fig.5.

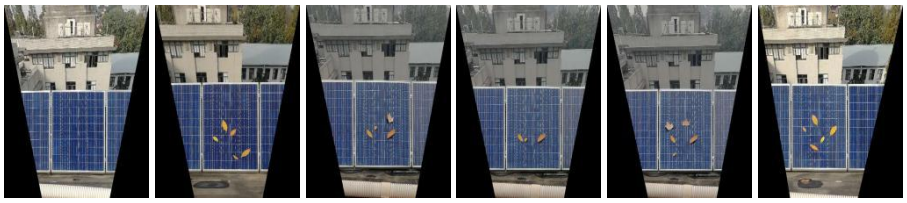

Fig. 8. The rectified visible images of PV modules

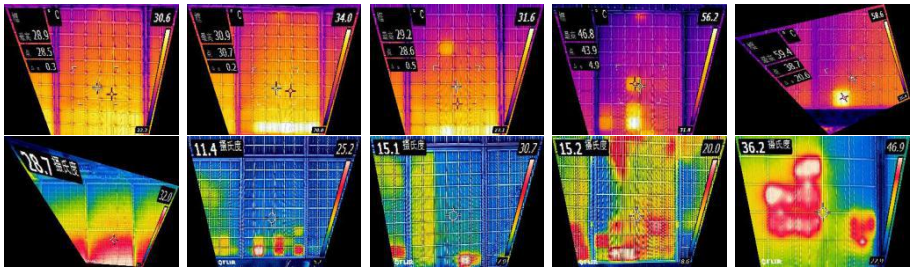

Fig. 9. The rectified IR images of PV modules

For a quantitative evaluation, we adopt the following metric:

$$error_1 = \frac{1}{N}\sum_{i=1}^{N}\sqrt{(\hat{a}_i - a_i)^2 + (\hat{b}_i - b_i)^2} \tag{15}$$

$$error_2 = \frac{1}{4N}\sum_{i=1}^{N}\sum_{c=1}^{4}\left|angle_{ic} - 90°\right| \tag{16}$$

Where $error_1$ is used to estimate the performance of affine rectification and $error_2$ is used for right angle estimation. N is the number of test samples: $N = 30$ for visible images and $N = 50$ for IR images. In equation (15), $(a, b, 1)^{\mathrm{T}}$ represents the line at infinity homogeneously. For each test case, a pair of vanishing points was manually annotated, giving the vanishing line. Thus, a_i, b_i are the ground truth parameters and $\hat{a}_i, \hat{b}_i$ is the calculated by affine rectification algorithm. In equation (16), $angle_{ic}(c = 1,2,3,4)$ are the angles of corners of the PV module after rectification for sample i.

We adopted TILT [18], TPS [19], and GCO [20] algorithms for comparison：

Table 1. The performance of visible images PV module rectification

Method / Metric	$error_1$	$error_2$
TILT	0.42	17.72
TPS	0.29	12.21
GCO	0.17	10.17
Proposed	0.06	3.32

Table 2. The performance of IR images PV module rectification

Method / Metric	$error_1$	$error_2$
TILT	0.46	18.33
TPS	0.32	14.27
GCO	0.16	10.68
Proposed	0.08	3.96

We can see clearly that the proposed method performs better than the other three methods for PV module rectification of visible images and IR images.

3.3 Anomalous area estimation

The area of shading in visible images are calculated, the results is shown in Table 3. The area is calculated by the shading pixels divided by the total PV pixels, represented in percentage. The ground truth is defined by manually specifying 4 corners of the PV modules.

Table 3. The area of shading in some visible images

	Image1	Image 2	Image 3	Image 4	Image 5	Error
Ground truth	3.15%	3.92%	2.66%	5.03%	4.70%	
Original	4.23%	2.86%	2.08%	4.00%	3.70%	16.47%
TILT	3.72%	3.88%	2.41%	4.67%	4.51%	6.33%
TPS	3.12%	3.85%	2.59%	4.85%	4.77%	2.09%
GCO	3.23%	3.81%	2.56%	4.88%	4.73%	6.16%
proposed	3.18%	3.96%	2.60%	4.97%	4.69%	1.04%

The area of hot spots in IR images of mono-crystalline silicon are calculated, the results is shown in Table 4.

Table 4. The area of hot spots in some IR images

	Image1	Image 2	Image 3	Image 4	Error
Ground truth	8.33%	5.00%	6.67%	1.67%	
Original	17.73%	9.17%	10.73%	2.39%	75.06%
TILT	8.15%	4.86%	6.79%	1.57%	3.19%
TPS	8.19%	4.88%	6.59%	1.76%	2.67%
GCO	8.21%	4.92%	6.82%	1.75%	3.47%
proposed	8.25%	4.96%	6.71%	1.72%	1.34%

4 Conclusion

A robust automatic method for removing projective distortion of photovoltaic modules from close shot images is proposed in this paper. Firstly, images are converted to gray scale, and edges are detected by Canny algorithm. Then, lines are detected by Hough transform, vanishing points are found by intersecting lines, and the line at infinity is recognized by vanishing points. Next, the projective transformation matrix is decomposed into an affine transformation matrix and a simple projective transformation matrix, which has only two degrees of freedom. Finally, affine rectification is achieved by computing this simple projective transformation matrix, and right angles are recovered by computing shear transformation matrix. The close-shot visible and infrared images are collected for experiments. The results show that the proposed method performs better than the other three methods for rectifying the PV modules in close-shot images.

Acknowledgement

This work was supported by the National Key Research and Development Program of China (Grant No. 2018YFB1500800), and by the National Natural Science Foundation of China (Grant No. 61773118, Grant No. 61703100, Grant No. 61973083, Grant No. 61802059), and by the Natural Science Foundation of Jiangsu (Grant No. BK20170692, Grant No. BK20180365), and by the Zhishan Young Scholar Program of Southeast University and the Fundamental Research Funds for the Central Universities (Grant No. 2242020R40119).

References

1. Bingol, Okan, Ozkaya, & Burcin. Analysis and comparison of different pv array configurations under partial shading conditions. Solar Energy. (2018).
2. Zhu, L. , Li, Q. , Chen, M. , Cao, K. , & Sun, Y. A simplified mathematical model for power output predicting of building integrated photovoltaic under partial shading conditions. Energy Conversion & Management, (2019). 180(JAN.), 831-843.
3. Niazi, K. A. K. , Akhtar, W. , Khan, H. A. , Yang, Y. , & Athar, S. . (2019). Hotspot diagnosis for solar photovoltaic modules using a naive bayes classifier. Solar Energy, 190, 34-43.
4. Dunderdale, C. , Brettenny, W. , Clohessy, C. , & Dyk, E. E. . (2019). Photovoltaic defect classification through thermal infrared imaging using a machine learning approach. Progress in Photovoltaics Research & Applications(3).
5. David Forsyth, Jean Ponce. Computer Vision: A Modern Approach. 2002
6. Richard Szeliski. Computer Vision: Algorithms and Applications. 2011
7. Bishop, C. M. . (2006). Pattern Recognition and Machine Learning (Information Science and Statistics). Springer-Verlag New York, Inc.
8. Hang Li. Statistical learning methods. Tsinghua University Press, Beijing (2012)

9. Ren, S. , He, K. , Girshick, R. , & Sun, J. . (2017). Faster r-cnn: towards real-time object detection with region proposal networks. IEEE Transactions on Pattern Analysis and Machine Intelligence, 39(6), 1137-1149.
10. Redmon, J. , Divvala, S. , Girshick, R. , & Farhadi, A. . (2015). You only look once: unified, real-time object detection.
11. Kaiming, H. , Georgia, G. , Piotr, D. , & Ross, G. . (2018). Mask r-cnn. IEEE Transactions on Pattern Analysis and Machine Intelligence.
12. Huang, Z. , Huang, L. , Gong, Y. , Huang, C. , & Wang, X. . (2019). Mask scoring r-cnn.
13. Chen, Liang-Chieh et al. "Encoder-Decoder with Atrous Separable Convolution for Semantic Image Segmentation." ECCV (2018).
14. Badrinarayanan, V. , Kendall, A. , & Cipolla, R. . (2017). Segnet: a deep convolutional encoder-decoder architecture for scene segmentation. IEEE Transactions on Pattern Analysis & Machine Intelligence.
15. Zhang, J. , Fang, S. , Ehinger, K. A. , Wei, H. , & Yang, J. . (2018). Hypergraph optimization for salient region detection based on foreground and background queries. IEEE Access, 6.
16. Zhang, J. , Ehinger, K. A. , Wei, H. , Zhang, K. , & Yang, J. . (2016). A novel graph-based optimization framework for salient object detection. Pattern Recognition, 64(C), 39-50.
17. Richard Hartley, Andrew Zisserman. Multiple view geometry in computer vision. 2000
18. Zhang, Z., Ganesh, A., Liang, X., & Ma, Y. (2012). TILT: Transform Invariant Low-Rank Textures. International Journal of Computer Vision, 99(1), 1-24.
19. Shi, B., Wang, X., Lyu, P., Yao, C., & Bai, X. (2016). Robust Scene Text Recognition with Automatic Rectification. computer vision and pattern recognition.
20. Ahmad, S., & Cheong, L. (2018). Robust Detection and Affine Rectification of Planar Homogeneous Texture for Scene Understanding. International Journal of Computer Vision, 126(8), 822-854.
21. Ahmad, S., & Cheong, L. (2016). Facilitating and Exploring Planar Homogeneous Texture for Indoor Scene Understanding. european conference on computer vision.
22. Pritts, J., Chum, O., & Matas, J. (2014). Detection, Rectification and Segmentation of Coplanar Repeated Patterns. computer vision and pattern recognition.
23. Shi, B., Yang, M., Wang, X., Lyu, P., Yao, C., & Bai, X. (2019). ASTER: An Attentional Scene Text Recognizer with Flexible Rectification. IEEE Transactions on Pattern Analysis and Machine Intelligence, 41(9), 2035-2048.
24. Canny, John, "A Computational Approach to Edge Detection," IEEE Transactions on Pattern Analysis and Machine Intelligence, Vol. PAMI-8, No. 6, 1986, pp. 679-698.
25. Lim, Jae S., Two-Dimensional Signal and Image Processing, Englewood Cliffs, NJ, Prentice Hall, 1990, pp. 478-488.
26. Parker, James R., Algorithms for Image Processing and Computer Vision, New York, John Wiley & Sons, Inc., 1997, pp. 23-29.
27. Duda, R. O. and P. E. Hart, "Use of the Hough Transformation to Detect Lines and Curves in Pictures," Comm. ACM, Vol. 15, pp. 11–15 (January, 1972)
28. Zhuang, X. (2016). Digital Affine Shear Transforms: Fast Realization and Applications in Image/Video Processing. Siam Journal on Imaging Sciences, 9(3), 1437-1466.
29. Liping Xie, Dacheng Tao, Haikun Wei, Early Expression Detection via Online Multi-instance Learning with Nonlinear Extension, IEEE Transactions on Neural Networks and Learning Systems (TNNLS), 2019, 30(5):1486-1496.
30. Liping Xie, Weili Guo, Haikun Wei, Yuanyan Tang, Dacheng Tao, Efficient Unsupervised Dimension Reduction for Streaming Multi-view Data, IEEE Transactions on Cybernetics, DOI: 10.1109/TCYB.2020.2996684.